ORIGINAL ARTICLE

eurosteel SHEFFIELD 2020

Ernst & Sohn A Wiley Brand

Simplified and advanced design for stainless steel members under concentrated transverse loading

Gabriel dos Santos, Leroy Gardner[1]

Correspondence

Dr. Gabriel dos Santos
University of Hertfordshire
School of Engineering and Computer Science
College Lane Campus
AL10 9AB Hatfield, UK
Email: g.santos@herts.ac.uk

Abstract

A comprehensive investigation into the behaviour of structural stainless steel members under concentrated transverse loading is presented in this paper. A total of 34 member tests and over 500 finite element simulations have been performed covering three types of concentrated transverse loading – internal one-flange, internal two-flange and end one-flange loading, three stainless steel grades – austenitic, duplex and ferritic and key influential parameters such as bearing length, web slenderness and beam span. The results have shown that existing design recommendations are conservative and that there is considerable scope for the development of more economical design guidance. New design equations are proposed that offer 10% to 20% improvements in capacity predictions over the current design formulae in EN 1993-1-4. These proposed design equations are to be included in the next revision of the European standards. An alternative design approach based on numerically generated reference loads – i.e. the plastic collapse and elastic buckling loads – in conjunction with strength curves, has also been proposed. This advanced FE-based design approach allows the extension of the design scope to non-standard cases, such as webs with partial depth stiffeners and members with web holes. The reliability of both design approaches has been successfully verified by statistical analysis.

Keywords

Concentrated transverse loading, Stainless steel, EN 1993-1-4, FE-based design approach, Reliability analysis.

1 Introduction

Structural steel members under concentrated transverse loading are encountered in a variety of situations such as primary beams under roof purlins, primary girders at bearing supports, columns in beam-to-column connections [1] and bridge girders during launching [2, 3]. Under this loading type, the members are subjected to non-uniform stress distributions, complex edge restraint conditions between the web and flanges and local yielding beneath the load [4]. Such conditions make the development of analytical formulations to accurately predict the ultimate resistances of members under concentrated loading non-trivial.

Experimental investigations carried out to determine the ultimate bearing resistances of steel members under concentrated transverse loading date back to 1946, when the first tests on cold-formed carbon steel members were reported [5]. Until recently, there have been very few tests on welded stainless steel I-section members subjected to concentrated transverse loading [6].

1. Imperial College London, Department of Civil and Environmental Engineering, London, UK.

Stainless steel has been increasingly widely used in structural engineering applications due to its combination of favourable structural properties, high recyclability and low maintenance costs associated with its excellent corrosion resistance. The most commonly used stainless steel types in construction are austenitic, duplex and ferritic stainless steels.

This article reports a comprehensive study carried out to investigate the behaviour of stainless steel members subjected to concentrated transverse loading. 34 member tests were carried out and over 500 finite element simulations have been performed covering three types of concentrated transverse loading – internal one-flange IOF (or Type 1), internal two-flange ITF (or Type 2) and end one-flange EOF (or Type 3) – as shown in Figure 1, where F_{Ed} is the applied concentrated load, s_s is the bearing length, a is the distance between web stiffeners, c is the distance between bearing plate and member end and b is the distance between bearing plates on opposing flanges. The results have shown that the existing design recommendations in EN 1993-1-4 [7] are conservative; hence, new design equations are proposed. An alternative design approach, based on numerically generated reference loads, namely the elastic buckling and plastic collapse loads under concentrated transverse forces, in conjunction with strength curves, has also been proposed. The reli-

ability of both proposed design approaches has been evaluated according to EN 1990 [8].

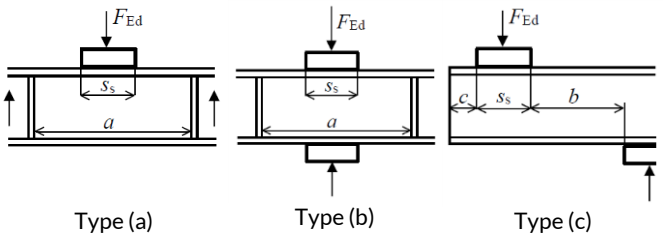

Figure 1 Types of concentrated transverse loading.

2 Experiments

2.1 Introduction

A total of 34 austenitic stainless steel member tests were carried out covering the three types of concentrated transverse loading shown in Figure 1; the tests provided valuable structural performance data and have been used to validate finite element models. A summary of the test results is presented in this section, with further information given in references [9, 10].

The specimens were fabricated from hot-rolled stainless steel plates which were laser-welded to form I-section shapes. Five cross-section sizes were examined: I102x68x5x5, I152x160x9x9, I150x75x710, I140x140x10x12 and I160x82x10x12. These cross-sections were formed from austenitic stainless steel of different grades: Grade EN 1.4571 for the first two cross-sections, Grade EN 1.4404 for the third and Grade EN 1.4307 for the fourth and fifth cross-sections. A comprehensive characterization of the tensile stress-strain properties of the cross-sections tested can be found in [11]; Table 1 provides a brief summary of the results, where E is the Young's modulus, f_y is the yield (0.2% proof) stress, f_u is the ultimate stress and ε_u is the ultimate strain. The coupons were extracted from the longitudinal direction of the members. For cross-sections comprising plates of the same thickness, a single coupon test was performed, while for those fabricated from plates of different thicknesses, two coupon tests were performed.

Table 1 Summary of material properties measured from tensile coupon tests [11].

Specimen	E (MPa)	f_y (MPa)	f_u (MPa)	ε_u %
I102 68x5x5	186800	222	580	50
I150x75x7x10 (Web)	197300	274	596	58
I150x75x7x10 (Flange)	197200	267	560	50
I152x160x6x9 (Web)	191400	272	586	50
I152x160x6x9 (Flange)	204700	227	561	52
I140x140x10x12 (Web)	186800	260	617	66
I140x140x10x12 (Flange)	193700	272	615	64
I160x82x10x12 (Web)	198500	264	618	53
I160x82x10x12 (Flange)	197500	286	619	52

Prior to the member tests, the dimensions and geometric imperfections of the specimens were measured. The initial imperfection measurements were taken as the maximum measured out-of-plane geometric imperfection along the web [9, 10].

The tests were designed to cover a wide range of structural responses and isolate the influence of key parameters such as web slenderness, bearing length, span and load position. The adopted test labelling system identifies the loading type (IOF, ITF or EOF), the nominal cross-section height (102 mm, 140 mm, 150 mm, 150 mm or 160 mm); for example, IOF-h102-I150-ss20 indicates a member under IOF loading with a cross-section height of 102 mm, a length of 500 mm and a bearing length of 20 mm.

2.1.1 Type (a) or Internal One-Flange (IOF) loading tests

The internal one-flange test setup consisted of a three-point bending configuration with the load applied through a bearing plate at mid-span, as shown in Figure 2. Two carbon steel plates were welded to the ends of the specimens and supported on rollers, which were configured to slide horizontally in response to the applied loading. The bearing plate, through which the loading was applied, had a roller welded to the top, which allowed rotation about the lateral axis, but no horizontal translation. Displacement control was adopted at a constant rate of 0.005 mm/sec. Figure 3 shows the IOF-I150 failed specimens of member lengths ranging from 150 mm to 450 mm subjected to concentrated load through a bearing length of 60 mm, all of which exhibited out-of-plane deformation of the web beneath the applied load and flange bending.

Figure 2 Experimental setup for IOF specimen tests.

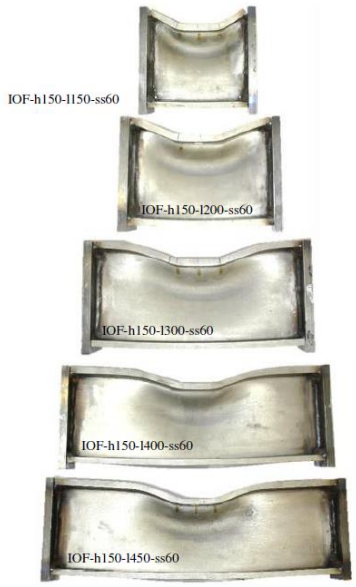

Figure 3 Failure modes of IOF-I150 under internal one-flange (IOF) loading [9].

2.1.2 Type (b) or Internal Two-Flange (ITF) loading tests

The internal two-flange (ITF) test setup shown in Figure 4 consists of a member subjected to two simultaneous transverse loads applied through two bearing plates, one positioned at the top flange and the other at the bottom flange. Both bearing plates had the same dimensions and were placed at the mid-span of the member. Carbon steel plates were welded to both ends of the test specimens. Similar to the IOF tests, the ITF tests were performed under displacement

control at a constant rate of 0.005 mm/sec. Figure 5 shows typical failure modes of the internal two-flange test specimens – i.e. mid-height out-of-plane web buckling failure together with significant local flange bending.

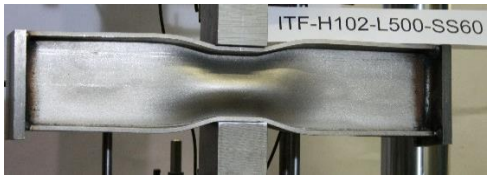

Figure 4 Experimental setup for ITF specimen tests.

Figure 5 Failure modes of ITF-I102 specimens under internal two-flange (ITF) loading [9].

2.1.3 Type (c) or End One-Flange (EOF) loading tests

The end one-flange loading test setup consisted of a three-point bending configuration with the load applied through the loading plate at the top flange of the beam, as shown in Figure 6. The loading plate length was kept constant at 100 mm for all tests. The bearing plate was positioned at one end of the member and lightly tack-welded to the bottom flange. Rollers were welded to the top of the loading plate and of the bearing plate to allow free in-plane rotation. A carbon steel end plate was welded to the opposite end of the member and supported on a roller. At both ends of the members, the rollers rested on plates that were configured to enable the beam to slide horizontally in response to the applied loading.

A load cell was positioned under the bearing plate to measure the reaction force at the critical support. Figure 7 shows the EOF-I160 failed specimens with varying *b* distances which corresponds to the distance between the free end of the member and the web stiffener. All specimens tested under EOF loading exhibited out-of-plane deformation of the web and flange bending at the bearing point.

Figure 6 Experimental setup for EOF specimen tests.

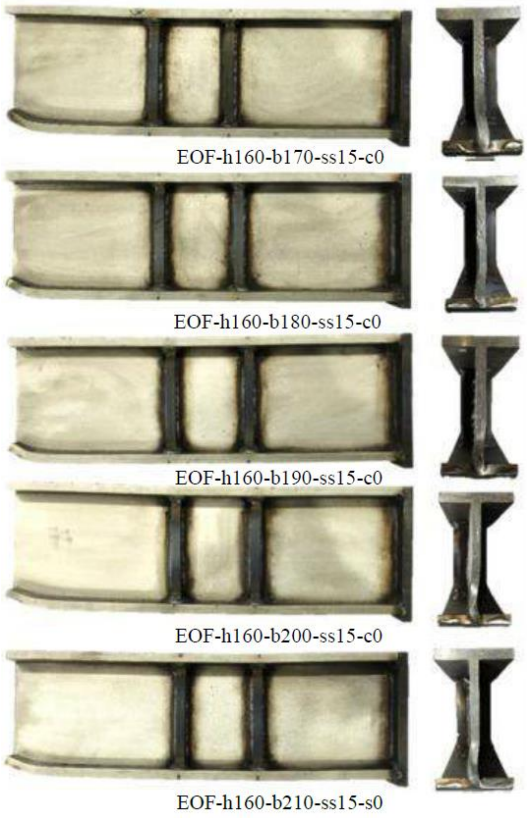

Figure 7 Failure modes of EOF-I160 specimens under end one-flange (EOF) loading [10].

3 Numerical modelling

Numerical models were developed using the finite element analysis software Abaqus [12]. Initially, the full load-displacement histories and failure modes obtained from the experiments were used to validate the numerical models and assess their sensitivity to various input parameters. Parametric studies were then carried out to extend the experimental database.

3.1 General assumptions and validation

The four-noded shell element with reduced integration, referred to as S4R [12], was used to mesh the beams and endplates, while the eight-noded linear solid element with reduced integration, referred to as C3D8R [12] was used to model the bearing plates. A uniform element size approximately equal to half of the web thickness of the considered I-sections was adopted for all features of the model, following a preliminary sensitivity study. For the austenitic stainless steel specimens, the measured engineering stress-strain curves obtained from tensile coupon tests [11] were converted into true stress log plastic strain curves before input into the finite element models. For the duplex and ferritic stainless steel specimens, the stress-strain behaviour was represented by the two-stage Ramberg-Osgood material model [13], with standardised key parameters of these material stress-strain curves used for the parametric studies [14].

The endplates were simulated as an elastic material behaviour with Young's modulus E = 210 000 MPa and Poisson's ratio ν = 0.3. The bearing plate was simulated as a rigid block by constraining all its degree of freedom to a reference point where the load was applied. The boundary conditions of the models were defined to reflect the three test setups. The interaction between the bearing plate and the

top (or bottom) flange of the I-sections was taken into account by defining surface-to-surface contact between the bearing plate (master surface) and the I-section flange (slave surface). A friction coefficient of 0.4 was used for the tangential contact properties while for the normal contact properties, a "hard" contact relationship was adopted.

Residual stresses were not incorporated into the models due to very low sensitivity of the response of I-section beams under concentrated transverse loading and bending [15]. A sensitivity study was carried out to investigate the influence of different imperfection magnitudes on the structural response. The best agreement between the test and finite element results was obtained for an imperfection amplitude of $t_w/500$ for all three loading cases; hence an amplitude of $t_w/500$ is adopted in the numerical models.

A geometrically and materially non-linear analysis with imperfections was conducted for each FE model to obtain the load-displacement curve and ultimate capacity of the member. The modified Riks solver was used to perform such analyses [12]. Excellent agreement was observed between the experimental and the numerical failure modes of specimens subjected to all three types of concentrated transverse loading. as shown in Figure 8.

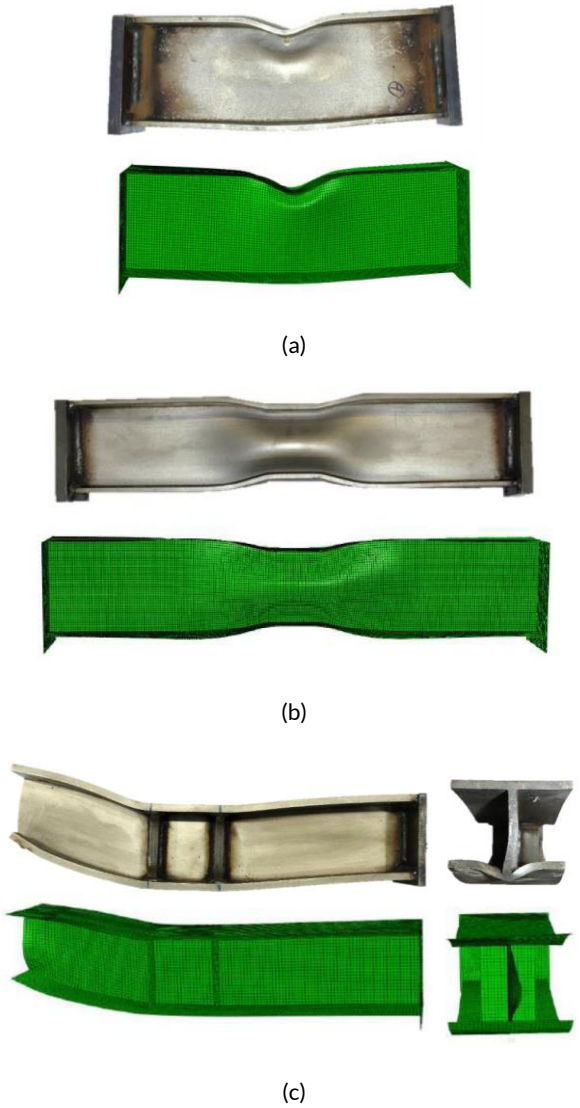

(a)

(b)

(c)

Figure 8 Experimental and numerical failure modes of specimen (a) IOF-h102-l300-ss12.5, (b) ITF-h102-l500-ss60 and (c) EOF-h140-b180-ss30-c0.

Typical numerical and experimental load versus web shortening responses for the three types of concentrated transverse loading investigated are shown in Figure 9. These comparisons show generally good agreement over the full load-deformation history, including initial stiffness, ultimate load and post-ultimate response. A summary of the validation results for all three loading cases is shown in Table 2, where $F_{u,FE}$ is the ultimate load from the finite element analysis and $F_{u,Test}$ is the ultimate load obtained from the test.

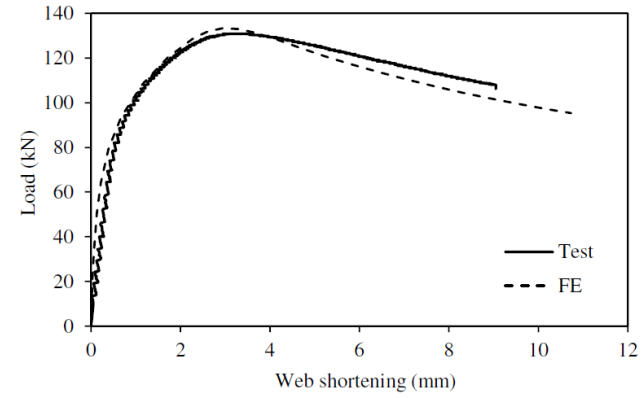

(a)

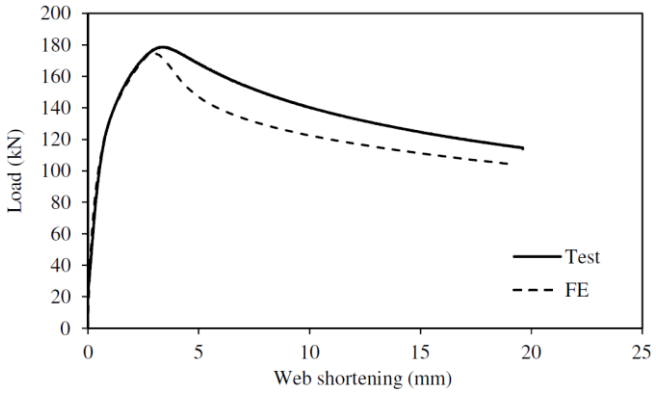

(b)

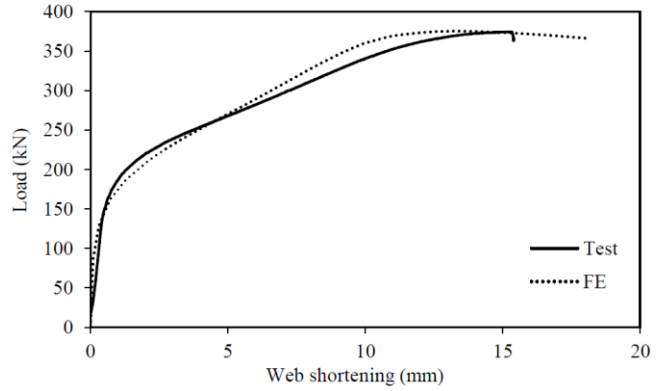

(c)

Figure 9 Experimental and numerical load-web shortening responses of the (a) IOF-h102-l300-ss15, (b) ITF-h102-l500-ss40 and (c) EOF-h140-b180-ss30-c0.

Table 2 Summary of comparisons between test and FE results for imperfection amplitude of $t_w/500$ [15].

Loading type	No. of tests	$F_{u,FE}/F_{u,Test}$	
		Mean	COV
Type (a), IOF [9]	16	1.01	0.04
Type (b), ITF [9]	8	0.96	0.04
Type (c), EOF [10]	10	1.01	0.13

4 Simplified design recommendations for stainless steel members under concentrated transverse loading

4.1 Review of experimental data and existing design methods

A total of 43 experiments on austenitic stainless steel I-section beams under three types of concentrated loading have been reported [6,9,10]; of these, 21 were performed under Type (a) loading, 8 under Type (b) loading and 14 under Type (c) loading. These data were used to assess the following existing design methods.

4.1.1 EN 1993-1-4 [7]

The current European design provisions for the resistance of stainless steel members to concentrated transverse loading simply refer to the design provisions for the resistance of carbon steel members in EN 1993-1-5 [16]. Originally proposed by Lagerqvist and Johansson [17], the design resistance to local failure under concentrated transverse loading F_{Rd} is presented as a function of the web yield strength f_{yw}, the web thickness t_w, an effective length L_{eff} and the partial safety factor γ_{M1}, as shown in Equation (1).

$$F_{\mathrm{Rd}} = \frac{f_{yw}\, L_{\mathrm{eff}}\, t_{\mathrm{w}}}{\gamma_{\mathrm{M1}}} \tag{1}$$

The effective length $L_{\mathrm{eff}} = \chi_{\mathrm{F}}\, l_{\mathrm{y}}$ is given by the product of the reduction factor χ_F and the effective loaded length, denoted l_y in general and $l_{y,a}$, $l_{y,b}$ or $l_{y,c}$ for loading Type (a), Type (b) or Type (c) respectively, as given by Equations (2) to (5), where s_s is the bearing length, t_f is the flange thickness, b_f is the flange width, f_{yf} is the flange yield strength, h_w is the web height and $m_{2,a}$, $m_{2,b}$ and $m_{2,c}$ are the m_2 factors for loading Types (a), (b) and (c), respectively.

$$l_{\mathrm{y,a}} = l_{\mathrm{y,b}} = l_{\mathrm{y},1}, l_{\mathrm{y,c}} = min\left(l_{\mathrm{y},1}, l_{\mathrm{y},2}, l_{\mathrm{y},3}\right) \tag{2}$$

where

$$l_{\mathrm{y},1} = s_{\mathrm{s}} + 2t_{\mathrm{f}}\left(1 + \sqrt{m_1 + m_2}\right) \le a,$$
$$l_{\mathrm{y},2} = l_{\mathrm{e}} + t_{\mathrm{f}}\sqrt{\frac{m_1}{2} + \left(\frac{l_{\mathrm{e}}}{t_{\mathrm{f}}}\right)^2 + m_2} \text{ and} \tag{3}$$
$$l_{\mathrm{y},3} = l_{\mathrm{e}} + t_{\mathrm{f}}\sqrt{m_1 + m_2}$$

in which

$$l_{\mathrm{e}} = \frac{k_{\mathrm{F}} E t_{\mathrm{w}}^2}{2 f_{\mathrm{yw}} h_{\mathrm{w}}} \le s_{\mathrm{s}} + c \tag{4}$$

and

$$m_1 = \frac{f_{\mathrm{yf}}\, b_{\mathrm{f}}}{f_{\mathrm{yw}}\, t_{\mathrm{w}}} \text{ and} \tag{5}$$

$$m_{2,\mathrm{a}} = m_{2,\mathrm{b}} = m_{2,\mathrm{c}} = \begin{cases} 0.02\left(\frac{h_{\mathrm{w}}}{t_{\mathrm{f}}}\right)^2 for \overline{\lambda}_{\mathrm{F}} > 0.5 \\ 0 for \overline{\lambda}_{\mathrm{F}} \le 0.5 \end{cases}$$

The reduction factor χ_F is function of the slenderness parameter $\overline{\lambda}_F$ which is equal to the square root of the ratio of the plastic load, given by Equation (8) to the elastic buckling load F_{cr} of the member under concentrated force.

$$\chi_{\mathrm{F}} = \frac{0.5}{\overline{\lambda}_{\mathrm{F}}} \le 1.0 \tag{6}$$

$$\overline{\lambda}_{\mathrm{F}} = \sqrt{\frac{F_{\mathrm{y}}}{F_{\mathrm{cr}}}} \tag{7}$$

$$F_{\mathrm{y}} = l_{\mathrm{y}} t_{\mathrm{w}} f_{\mathrm{yw}} \tag{8}$$

The elastic buckling load F_{cr} is determined from Equation (9) where E is the Young's modulus, k_f is the buckling coefficient dependent on the type of transverse loading, as given by Equation (10), a is the distance between web stiffeners and c is the distance between the bearing load and the member end.

$$F_{\mathrm{cr}} = 0.9 k_{\mathrm{F}} E \frac{t_{\mathrm{w}}^3}{h_{\mathrm{w}}} \tag{9}$$

where

$$k_{\mathrm{F}} = \begin{cases} 6 + 2\left(\frac{h_{\mathrm{w}}}{a}\right)^2 \text{ for Type}(a) \text{ loading} \\ 3.5 + 2\left(\frac{h_{\mathrm{w}}}{a}\right)^2 \text{ for Type}(b) \text{ loading} \\ 2 + 6\left(\frac{s_{\mathrm{s}} + c}{h_{\mathrm{w}}}\right) \le 6 \text{ for Type}(c) \text{ loading} \end{cases} \tag{10}$$

In the case of members subjected to concentrated transverse loading F plus bending moment M, for example under Type (a) loading, the F-M interaction is considered through Equation (11), where F_{Ed} is the applied concentrated transverse force, F_{Rd} is the design resistance to concentrated transverse force given by Equation (1), M_{Ed} is the applied bending moment and $M_{pl,Rd}$ is the plastic bending moment resistance of the cross-section, regardless of its classification.

$$\frac{F_{\mathrm{Ed}}}{F_{\mathrm{Rd}}} + 0.8\frac{M_{\mathrm{Ed}}}{M_{\mathrm{pl,Rd}}} \le 1.4 \tag{11}$$

4.1.2 Recent design proposals for carbon steel members

Following a series of studies on the behaviour of carbon steel I-beams subjected to concentrated transverse loading [18-21], two main modifications were proposed to the existing effective loaded length l_y formulae, i.e. Equations (2) to (5), to simplify and improve the prediction of ultimate load-carrying capacity: (i) removal of the m_2 term for Type (a) and Type (b) loading cases [18 - 20] and (ii) removal of the yield strength ratio from the m_1 term for all loading types [21], resulting in the replacement of Equation (5) by Equation (12).

$$m_1 = \frac{b_{\mathrm{f}}}{t_{\mathrm{w}}}, m_{2,\mathrm{a}} = m_{2,\mathrm{b}} = 0 \text{ and}$$
$$m_{2,\mathrm{c}} = \begin{cases} 0.02\left(\frac{h_{\mathrm{w}}}{t_{\mathrm{f}}}\right)^2 for \overline{\lambda}_{\mathrm{F}} > 0.5 \\ 0 for \overline{\lambda}_{\mathrm{F}} \le 0.5 \end{cases} \tag{12}$$

A new expression for the buckling reduction factor χ_F was also proposed [22] to replace the existing plate-like resistance function of Equations (6) to (10) by a column-like resistance function given by Equations (13) and (14), with the imperfection factor α_{F0} = 0.75 and the plateau length $\overline{\lambda}_{F0} = 0.50$. These described design proposals are due to be incorporated into the next revision of EN 1993-1-5 [16].

$$\chi_F = \frac{1}{\phi_F + \sqrt{\phi_F^2 - \overline{\lambda}_F}} \text{ but } \chi_F \leq 1.0 \tag{13}$$

where

$$\phi_F = \frac{1}{2}\left[1 + \alpha_{F0}\left(\overline{\lambda}_F - \overline{\lambda}_{F0}\right) + \overline{\lambda}_F\right] \tag{14}$$

4.2 Assessment of existing design methods

The available test and numerical data are used to evaluate the accuracy of the design provisions described in the previous section. The accuracy of the design predictions is evaluated by comparing the numerical or test failure F_u with the ultimate load predicted by the design procedure $F_{Rd,pred}$ for austenitic, duplex and ferritic stainless steel members under three types of concentrated loading. Only cases where the critical design check was based on concentrated transverse loading have been considered from this point onwards. To account for the combined bending moment and concentrated loading that arises under Type (a) loading, the design interaction curve given by Equation (11) was used. Note that all partial safety factors were set equal to unity for comparison purposes.

4.2.1 EN 1993-1-4 [7]

Conservative results were obtained for all three loading types when considering the design rules given in EN 1993-1-4 against the available test and numerical data. An average underprediction of capacity of approximately 50% for Types (a) and (c) loading and 75% for Type (b) loading were obtained [15]. Similar results were obtained by Selen [6] – i.e. an average of 34% underprediction of capacity for Type (a) loading and 46% for Type (c) loading. The underpredictions of capacity are observed throughout the slenderness range and are associated with the inherent difference in stress-strain behaviour of stainless steel and carbon steel. The underpredictions of capacity are particularly evident in the stocky slenderness range. The test and numerical data on stainless steel members under concentrated loading are plotted in terms of the buckling reduction factor versus slenderness in Figure 10.

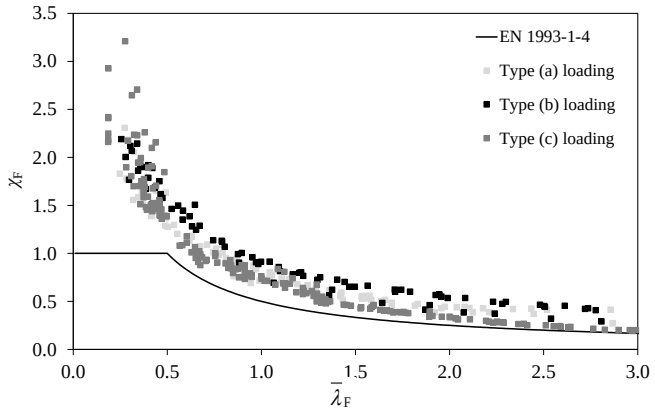

Figure 10 Comparison of test and numerical data with EN 1993-1-4 design resistance for stainless steel members under concentraterd transverse loading.

4.2.2 Recent design proposal for carbon steel members

The recently proposed design rules for carbon steel members subjected to concentrated transverse loading [21] provides a slight improvement in capacity prediction accuracy, particularly for higher values of slenderness [22]. However, there still remains considerable scope for further improvements in the ultimate capacity predictions of stainless steel members subjected to concentrated loading. The test and numerical data on stainless steel members subjected to concentrated transverse loading are plotted in terms of reduction factor versus slenderness in Figure 11.

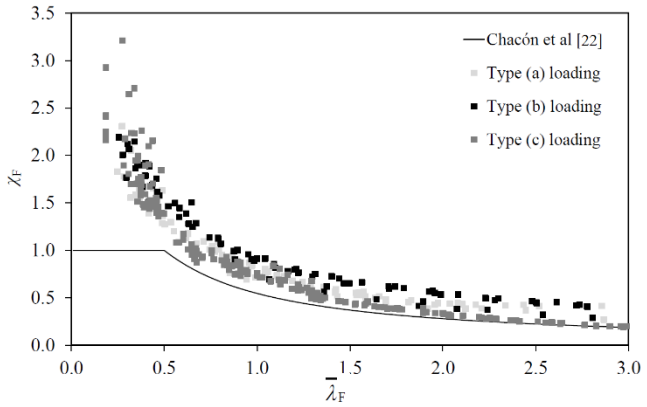

Figure 11 Comparison of test and numerical data on stainless steel members with recently proposed design resistance curve for carbon steel members under concentrated transverse loading.

4.3 New proposed design rules

The improved design rules proposed herein for stainless steel members under concentrated transverse loading are based on the recent design proposal for carbon steel members presented in Section 4.1.2. The adoption of the new resistance function given by Equations (13) and (14) ensures compatibility of design approach between stainless steel and carbon steel members, but with the α_{F0} and $\overline{\lambda}_{F0}$ parameters calibrated for stainless steel. The calibration has been carried out based on data from 39 test results and 369 numerical results reported by dos Santos and Gardner [15].

In the new design proposal for stainless steel members, the buckling reduction factor χ_F is given by Equation (13), with the parameter ϕ_F defined by Equation (14) and slenderness $\overline{\lambda}_F$ given by Equation (7). The critical buckling load F_{cr} and the buckling coefficient k_F for each loading type are given by Equation (9) whereas the plastic collapse load F_y is given by Equation (8). The effective loaded length l_y is given by Equations (2) to (4), with values of m_1 and m_2 given by Equation (12). Following analysis of the test and numerical data, new imperfection factor α_{F0} and plateau length $\overline{\lambda}_{F0}$ values are proposed in Table 3 according to the loading type and stainless steel grade.

Table 3 Values of α_{F0} and $\overline{\lambda}_{F0}$ for new proposed design approach [15].

Loading type	Austenitic and Duplex		Ferritic	
	α_{F0}	$\overline{\lambda}_{F0}$	α_{F0}	$\overline{\lambda}_{F0}$
Type (a), IOF [9] Type (b), ITF [9]	0.60	0.60	0.30	0.65
Type (c), EOF [10]	0.75	0.50	0.75	0.50

The new design proposal brings consistent improvements for Type (a) and Type (b) loading, and similar results for Type (c) loading. A

comparison of the EN 1993-1-4, Chacón et al [22] and the new proposed strength curves are presented below, where the data are presented in groups of the same proposed α_{F0} and $\overline{\lambda}_{F0}$ values: austenitic and duplex stainless steel members under Type (a) and Type (b) loading are shown in Figure 12, ferritic stainless steel members under Type (a) and Type (b) loading are shown in Figure 13 and all stainless steel members under Type (c) loading are shown in Figure 14.

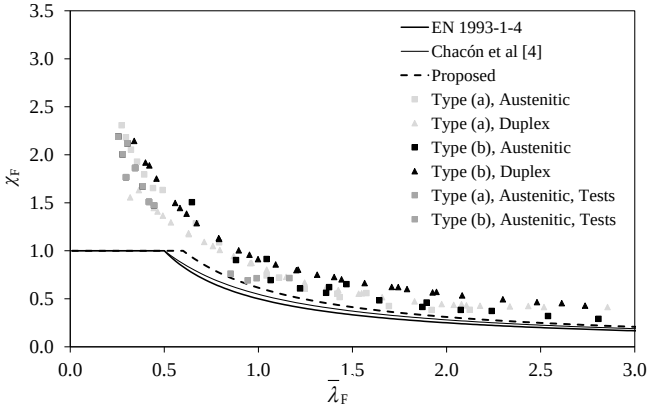

Figure 12 Comparison of test and numerical data with proposed design resistance equations for austenitic and duplex stainless steel members under Type (a) and Type (b) concentrated loading.

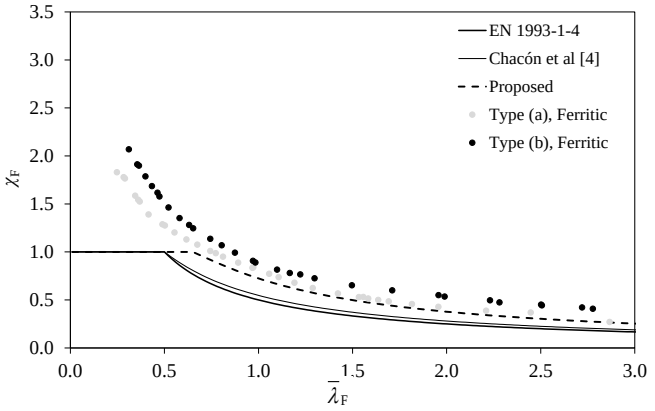

Figure 13 Comparison of test and numerical data with proposed design resistance equations for ferritic stainless steel members under Type (a) and Type (b) concentrated loading.

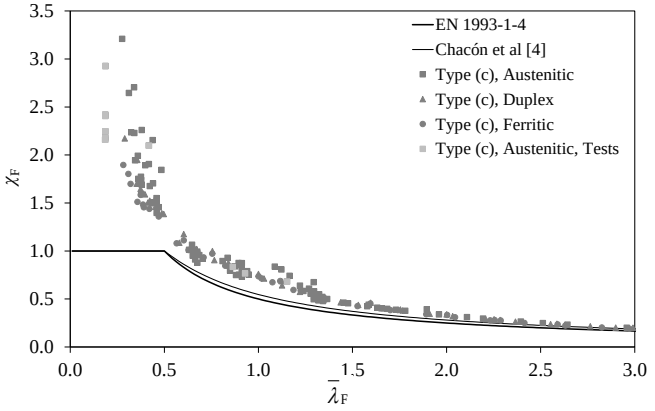

Figure 14 Comparison of test and numerical data with proposed design resistance equations for stainless steel members under Type (c) concentrated loading.

The members subjected to Type (a) loading with $M_u \geq 0.5M_{pl,Rd}$ have not been included in the comparisons presented thus far to allow the effect of concentrated transverse loading to be assessed in isolation. These data points are assessed using the interaction curve given by Equation (11), as presented in Figure 15, where F_u and M_u are the ultimate load and moment respectively from the Type (a) loading tests and numerical models, $F_{u,prop}$ is the ultimate load predicted using the proposals made in this section and $M_{pl,Rd}$ is the plastic bending resistance of the cross-section, regardless of its classification. The design interaction curve may be seen to provide consistently safe-sided predictions with the proposed end-point for resistance to concentrated transverse loading $F_{u,prop}$.

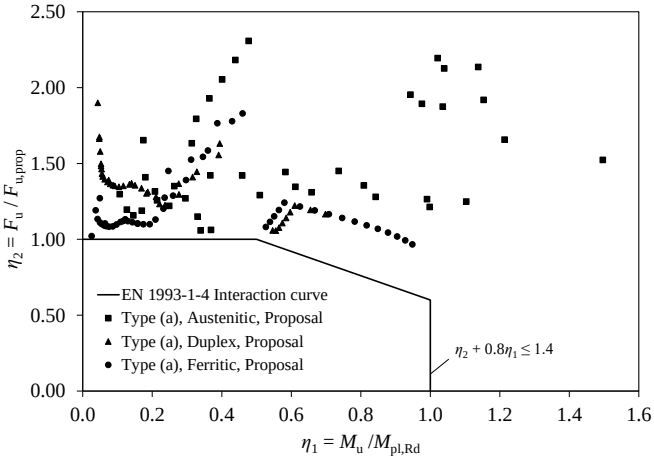

Figure 15 Interaction curve adopted in EN 1993-1-4 for Type (a) loading but with new proposed end point $F_{u,prop}$ together with numerical data.

Overall the proposed design rules are consistent with the new provisions for carbon steel sectionc subjected to concentrated transverse loading due to be incorporated into the next revision of EN 1993-1-5, feature new imperfection factors and plateau length values that reflect the particular characteristics of stainless steel and result in average enhancements in efficiency of about 10% for Type (a) loading and 20% for Type (b) loading.

4.4 Reliability analysis

An assessment of the reliability of the proposed design equations for predicting the ultimate capacity of stainless steel members under concentrated transverse forces, as set out in Section 4.3, was performed according to Annex D of EN 1990 [8]. Reliability analyses were carried out on 12 groups of data: one for each material grade, i.e. austenitic, duplex and ferritic stainless steel, and for each loading type, i.e. Type (a) loading with $M_u \geq 0.5\ M_{Rd}$, Type (a) loading with $M_u < 0.5\ M_{Rd}$, Type (b) loading and Type (c) loading.

The procedure described in Annex D of EN 1990 [8] requires the assessment of a resistance function F_{Rd} containing only independent variables – i.e. web thickness t_w and web yield stress f_{yw}. By considering the variability of each independent variable, as well as accounting for variability generated by the use of numerical data and the amount of data used, it was found that the proposed design equations presented in Section 4.3, with coefficients presented in Table 3, can be safely applied to the design of stainless steel members under concentrated transverse loading with a partial factor γ_{M1} equal to 1.1 [15].

5 Advanced FE-based approach for stainless steel members under concentrated transverse loading

5.1 Introduction

Steel structural design codes commonly adopt design methods based on two key reference loads: the plastic collapse load and the

elastic buckling load, from which the element slenderness and hence the element resistance can be determined. These reference loads are typically determined using simplified analytical expressions e.g. the squash load and the Euler load of a column. However, for the more complex loading conditions, boundary conditions and failure mechanisms associated with concentrated transverse loading, obtaining accurate values for these reference loads from simplified analytical expressions is less straightforward. Hence, an advanced FE-based design method for stainless steel members subjected to concentrated transverse loading is proposed herein. In this method, both reference loads are obtained from finite element analysis, which allows not only more accurate values for the reference loads to be obtained for the common cases covered by analytical expressions, but also straightforward extension of the scope of the design approach to non-standard cases, such as webs with partial depth stiffeners.

5.2 Modelling assumptions and validation

A numerical modelling programme has been carried out to obtain the key reference loads for the FE-based design of stainless steel I-beams under concentrated transverse loading – i.e. the plastic collapse load and the elastic buckling load. The finite element software Abaqus [12] was adopted to carry out the numerical analysis. The numerical results generated to assess the design method proposed in Section 4.3 were used for the ultimate capacity of members F_u under concentrated transverse loading. Further FE modelling has been performed to obtain the plastic collapse load $F_{pl,FE}$ according to the validated methodology presented by dos Santos et al [23], and the elastic buckling load $F_{cr,FE}$ from linear buckling analysis corresponding to each of the parametric cases.

A comprehensive description of the finite element models used to obtain the plastic collapse load has been presented by dos Santos et al [23] and in Section 3 of this article; hence, only further relevant information of key features of the materially non-linear analysis used to obtain $F_{pl,FE}$, and linear buckling analysis used to obtain $F_{cr,FE}$, are presented here.

Materially non-linear analysis (MNA) and linear buckling analysis (LBA) were performed for each case considered in Section 4, excluding those with bearing lengths longer than 50 mm. MNA adopts an elastic perfectly plastic stress-strain model defined by the Young's modulus E and the yield strength f_y, whereas the LBA adopts a linear elastic material model defined the Young's modulus E.

The plastic collapse load $F_{y,FE}$ from a materially non-linear analysis (MNA) is defined herein as the load at which the tangent stiffness of the load-displacement curve achieves 1% of the initial tangent stiffness. Further details on the numerical procedure to obtain the plastic collapse load from a materially non-linear analysis (MNA) have been presented by dos Santos et al [23]. The elastic buckling load $F_{cr,FE}$ obtained from a linear elastic buckling analysis corresponds to the first eigenvalue.

5.3 Standard and non-standard cases

For the standard cases, such those investigated thus far in this article (Figure 1), a total of 1005 FE-models were run, of which 335 geometrically and materially non-linear analyses with imperfections (GMNIA) to obtain the ultimate loads F_u, 335 were materially non-linear analysis (MNA) to obtain the plastic collapse loads $F_{pl,FE}$ and 335 were linear buckling analysis (LBA) to obtain the elastic buckling loads $F_{cr,FE}$.

To demonstrate the applicability of the proposed design equations to non-standard cases, members with partial web stiffeners were considered. All modelled cross-sections had a web height h_w of 410 mm, a flange width b_f of 150 mm, a flange thickness t_f of 20 mm, a bearing length s_s of 20 mm, a member length L equal to 600 mm, a web stiffener thickness $t_{ws} = t_w$ and a web stiffener height h_{ws} varying from 10% to 30% of the web height. The cross-section web thickness was also varied to cover web slendernesses values from 0.40 to 2.70. Only duplex stainless steel beams under Type (a) loading were investigated herein due to the wide application of duplex stainless steel in structural elements of bridge structures, frequently subjected to concentrated transverse loading. A typical FE model of a member with a partial-depth web stiffener subjected to Type (a) loading and its deformed shape obtained from geometrically and materially non-linear analysis with imperfections (GMNIA) is shown in Figure 16.

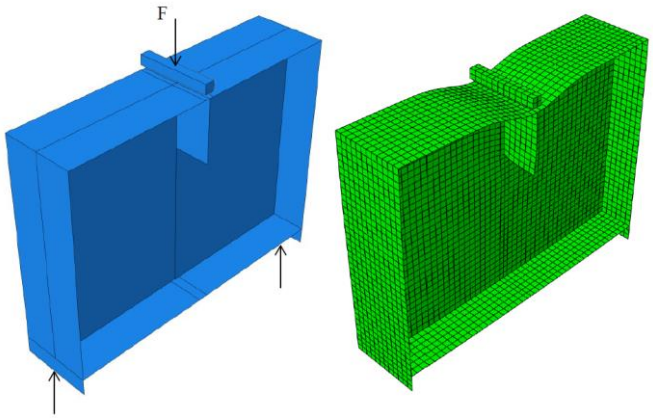

Figure 16 Finite element model with a partial-depth web stiffener of 30% of the web height and corresponding deformed shape under Type (a) loading.

5.4 Proposed FE-based design method

The advanced FE-based design proposal presented herein is based on the two key reference loads – plastic collapse loads $F_{pl,FE}$ and elastic buckling loads $F_{cr,FE}$ – obtained through a materially non-linear analysis (MNA) and a linear buckling analysis (LBA), respectively. Hence, the ultimate resistance F_{Rd} of a stainless steel member under concentrated transverse loading is given by the product of a buckling reduction factor χ_F and the numerically obtained plastic collapse load $F_{pl,FE}$ as shown in Equation 15.

$$F_{Rd} = \chi_F F_{pl,FE} \tag{15}$$

The buckling reduction factor (i.e. the strength curve) is defined using the same form of equation adopted for the traditional design approach – i.e. Equations 13 and 14, but with the parameters α_{F0} and $\overline{\lambda}_{F0}$ re-calibrated based on the numerically derived slenderness, termed $\overline{\lambda}_{F,FE}$ in place of $\overline{\lambda}_F$. $\overline{\lambda}_{F,FE}$ is defined by Equation 16 where $F_{cr,FE}$ is the elastic buckling load obtained from a linear buckling analysis and $F_{pl,FE}$ is the plastic collapse load obtained according to the tangent stiffness plot (TS Plot) method presented by dos Santos et al [23] – i.e. the plastic collapse load is defined as the load value at which the tangent stiffness in the load-displacement curve of an MNA becomes 1% of its initial elastic stiffness. No extrapolation techniques to obtain the plastic collapse load, such as those presented by dos Santos et al [23] were required herein.

$$\overline{\lambda}_{F,FE} = \sqrt{\frac{F_{pl,FE}}{F_{cr,FE}}} \tag{16}$$

Following calibration of the resistance function against the test and

numerical data, a new set of imperfection factors and plateau length values are proposed in Table 4.

Table 4 Values of α_{F0} and $\overline{\lambda}_{F0}$ for advanced FE-based design proposal.

Loading type	α_{F0}	$\overline{\lambda}_{F0}$
Type (a), IOF [9]	0.40	0.50
Type (b), ITF [9]	0.10	0.85
Type (c), EOF [10]	1.05	0.80

A comparison between the EN 1993-1-4 [7] and the new proposed strength curves using FE-based slenderness $\overline{\lambda}_{F,FE}$ are presented by loading type in Figures 17 to 19.

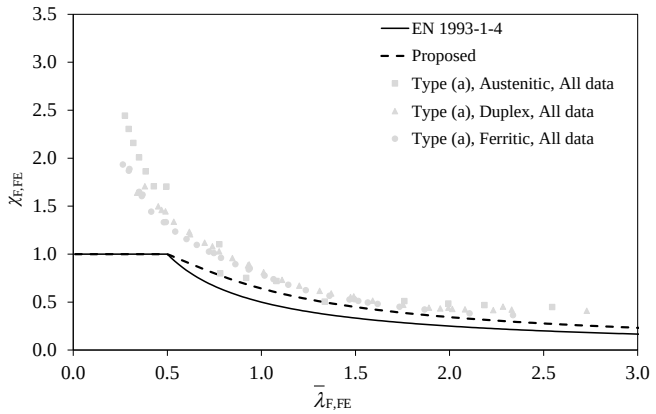

Figure 17 Comparison of test and numerical data with FE-based resistance equations for stainless steel members under Type (a) concentrated loading.

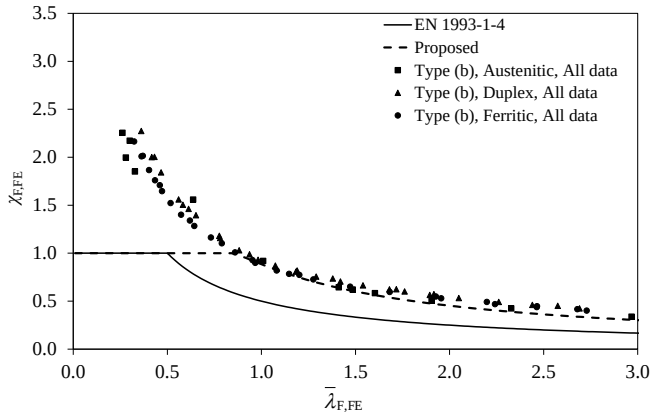

Figure 18 Comparison of test and numerical data with FE-based resistance equations for stainless steel members under Type (b) concentrated loading.

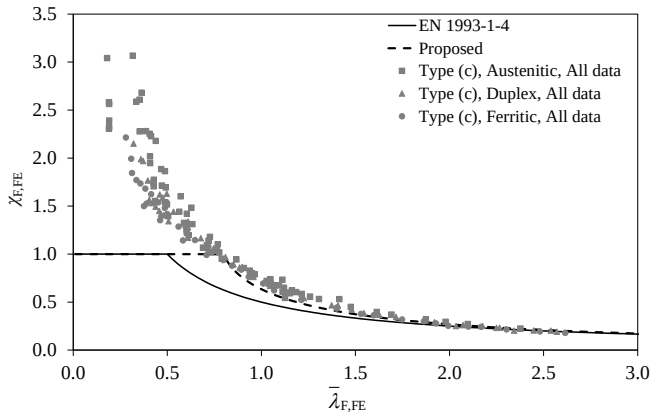

Figure 19 Comparison of test and numerical data with FE-based resistance equations for stainless steel members under Type (c) concentrated loading.

Overall, the FE-based design proposal for stainless steel members under concentrated transverse loading, utilising numerical estimates for the key reference loads, results in average enhancements in efficiency of 17% in comparison to the design method presented in Section 4, with a 31% enhancement for Type (b) loading. Relative to both the current Eurocode design approach and the new design procedure presented in Section 4, the mean predictions are more accurate and the scatter is reduced. A further benefit of the proposed FE-based approach is the applicability to non-standard cases, as presented in the following subsection.

5.5 Application to members with partial-depth web stiffeners

The FE-based design approach for stainless steel members under concentrated transverse loading has been considered thus far for members without web stiffeners under the bearing load. However, the FE-based design approach allows the analysis of non-standard cases, such as members with partial-depth web stiffeners. A comparison between the proposed strength curve for Type (a) loading and duplex stainless steel members without web stiffeners and with partial-depth web stiffeners is presented in Figure 20. The figure shows that the data for members with and without web stiffeners, indicating that the proposed design expressions for Type (a) members without web stiffeners may be safely applied to the design of members with partial-depth web stiffeners. This indicates the general applicability and flexibility of the proposed method and sets foundations for further studies.

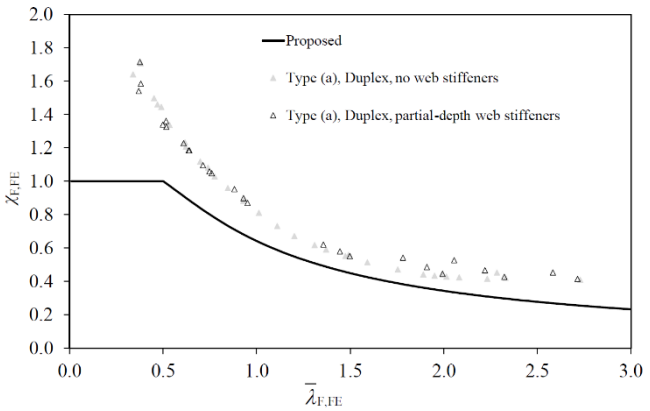

Figure 20 Comparison of numerical data for duplex stainless steel members under Type (a) loading with and without web stiffeners and design resistance equation proposed in Section 4.

5.6 Reliability analysis

Statistical analysis was carried out to assess the reliability of the proposed FE-based equations for predicting the ultimate capacity of stainless steel members under concentrated transverse forces according to Annex D of EN 1990 [8]. Reliability analyses were performed on 12 groups of data, divided by loading type and material type. Further details on the coefficients of variation for the web yield strength and web thickness, material overstrength factors and variability related to the numerical results can be found in dos Santos [24]. The required values for the partial safety factor γ_{M1} are, on average, lower than 1.10, which is the partial safety factor adopted in EN 1993-1-4 for the design of stainless steel members under concentrated loading. Therefore, the proposed design equations with a partial safety factor of 1.10 can be safely applied to the design of stainless steel members under concentrated transverse loading.

6 Conclusions

This article presents a comprehensive study into the design of stainless steel members subjected to concentrated transverse loading, including physical laboratory experimentation, numerical modelling, development of simplified design rules according to EN 1993-1-4, advanced design rules based on finite element simulations and reliability analyses. The proposed simplified method, based on EN 1993-1-4, resulted in clear improvements in the ultimate capacity predictions relative to the test and FE results when compared with the current Eurocode design provisions. The advanced design method, an FE-based design procedure, which utilises numerical analysis to determine two key reference loads – the plastic collapse load and the elastic buckling load, provides a reliable alternative design method to the Eurocode provisions with an average enhancement in efficiency of 17% in comparison to the proposed simplified method. The flexibility and general applicability of the FE-based design method warrants further investigation and verification, particularly to steel and stainless steel members with non-standard features such as partial-depth web stiffeners, web holes and tapered beams. The wider applicability and gains in accuracy of the proposed method compared to traditional design procedures may justify the greater sophistication.

References

[1] Graham, J.D., Sherbourne, A.N., Kabbaz, R.N., and Jensen, C.D. (1959) *Welded interior beam-to-column connections.* American Institute of Steel Construction, AISC.

[2] Granath, P. and Lagerqvist, O. (1999) Behaviour of girder webs subjected to patch loading. Journal of Constructional Steel Research, 50(1), 49-69.

[3] Chacón, R.; Herrera, J. and Fargier-Gabaldon, L. (2017) Improved design of transversally stiffened steel plate girders subjected to patch loading. Engineering Structures, 150(1), 774-785.

[4] Macdonald, M.; Heiyantuduwa, M.A.; Harrison, D.K.; Bailey, R. and Rhodes, J. (2005) Literature review of web crippling behaviour. 2nd Scottish Conference for Postgraduate Researchers of the Built and Natural Environment. Rotterdam, Netherlands.

[5] Winter, G. and Pian, R.H.J. (1946) Crushing strength of thin steel webs. Engineering Experiment Station, Bulletin No. 35 (Part 1), 1-24.

[6] Sélen, E. (2000) Work package 3.5 - Final report - Web crippling. Report to the ECSC Project - Development of the use of stainless steel in construction. Contract No. 7210-SA/903, Lulea University of Technology, 2000.

[7] EN 1993-1-4. (2006) Eurocode 3: Design of steel structures - Part 1.4: General rules - Supplementary rules for stainless steels. European Committee for Standardization (CEN). Brussels, Belgium.

[8] EN 1990. (2002) Eurocode: Basis of structural design. European Committee for Standardization (CEN). Brussels, Belgium.

[9] dos Santos, G.B.; Gardner, L. and Kucukler, M. (2018) Experimental and numerical study of stainless steel I-sections under concentrated internal one-flange and internal two-flange loading. Engineering Structures, 175, 355-370.

[10] dos Santos, G.B.; Gardner, L. (2019) Testing and numerical analysis of stainless steel I-sections under concentrated end-one-flange loading. Journal of Constructional Steel Research, 157, 271-281.

[11] Gardner, L., Bu, Y. and Theofanous, M. (2016) Laser-welded stainless steel I-sections: Residual stress measurements and column buckling tests. Engineering Structures, 127, 536-548.

[12] ABAQUS. (2014) Abaqus version 6.14. SIMULIA - Dassault Systèmes. Software.

[13] Arrayago, I., Real, E. and Gardner, L. (2015) Description of stress-strain curves for stainless steel alloys. Materials and Design, 87, 540-552.

[14] Afshan, S. Zhao, O. and Gardner, L. (2019) Standardised material properties for numerical parametric studies of stainless steel structures and buckling curves for tubular columns. Journal of Constructional Steel Research, 152, 2-11.

[15] dos Santos, G.; Gardner, L. (2020) Design recommendations for stainless steel I-sections under concentrated transverse loading. Engineering Structures, 204, 109810.

[16] EN 1993-1-5. (2006) Eurocode 3: Design of steel structures - Part 1-5: Plated structural elements. European Committee for Standardization (CEN). Brussels, Belgium.

[17] Lagerqvist, O. And Johansson, B. (1996) Resistance of I-girders to concentrated loads. Journal of Constructional Steel Research, 39(2), 87-119.

[18] Davaine, L. (2005) Formulation de la résistance au lancement d'une âme métallique de pont raidie longitudinalement, Institut National des Sciences Appliquées. PhD thesis.

[19] Gozzi, J. (2007) Patch loading resistance of plated girders - Ultimate and serviceability limit state. Luleå University of Technology. PhD thesis.

[20] Clarin, M. (2007) Plate buckling resistance – Patch loading of longitudinally stiffened webs and local buckling. Luleå University of Technology. PhD thesis.

[21] Chacón, R.; Mirambell, E. and Real, E. (2010) Hybrid steel plate girders subjected to patch loading, Part 2: Design proposal. Journal of Constructional Steel Research, 66, 709-715

[22] Chacón, R.; Braun, B.; Kuhlmann, U. and Mirambell, E. (2012) Statistical evaluation of the new resistance model for steel plate girders subjected to patch loading. Steel Construction, 5(1).

[23] dos Santos, G.B.; Gardner, L. and Kucukler, M. (2018) A method for the numerical derivation of plastic collapse loads. Thin-Walled Structures, 124, 258-277.

[24] dos Santos, G.B. (2019) Behaviour and design of structural stainless steel members under concentrated transverse forces. Imperial College London. PhD thesis.